Journal Name

ARTICLE

Solvent-Controlled Syntheses of Mixed-Alkali-Metal Borates Exhibiting UV Nonlinear Optical Properties

Received 00th January 20xx,
Accepted 00th January 20xx

DOI: 10.1039/x0xx00000x

www.rsc.org/

Chao Wu,[a] Longhua Li,[a] Junling Song,[a] Gang Yang,[a] Mark G. Humphrey[b] and Chi Zhang*[a]

The mixed-alkali-metal borates $NaK(B_5O_8)(OH)\cdot H_2O$ (**1**), $NaK_6[(B_4O_5)(OH)_4]_3(OH)\cdot C_2H_5OH$ (**2**) and $Na_{0.33}K_{1.67}(B_4O_5)(OH)_4\cdot 3H_2O$ (**3**) have been solvothermally synthesized using various polar organic solvents. Compounds **1** and **2** crystallize in the centrosymmetric space groups $P\bar{1}$ and $R\bar{3}c$, respectively. The structure of **1** features a 2D-layered framework constructed by $[B_5O_{11}]^{7-}$ primary building units in the *ab* plane, extending to a 3D framework linked by K^+ and Na^+ cations, while the structure of **2** can be described as isolated $[B_4O_9]^{6-}$ primary building units connected by H-bonding interactions and K-O and Na-O bonds, forming a 3D supramolecular framework. Compound **3** crystallizes in the acentric space group $P\bar{6}2c$, and its UV nonlinear optical properties have been investigated for the first time. Second-harmonic generation (SHG) measurements show that **3** is type-I phase-matching, with a moderate SHG response ca. 0.94 times that of KH_2PO_4. The cut-off edge of **3** is 242 nm, which suggests that **3** is a potential UV NLO material. Density functional theory calculations have been employed on **3** to rationalize its band structure and electron density as well as the density of states.

Introduction

The development of second-order nonlinear optical (NLO) materials is of key importance for practical applications such as frequency conversion, electro-optical switching, nano-micro mechanical machining, and signal communication,[1-2] and as NLO-active crystals that can be used in the UV and infrared (IR) spectral regions.[3-5] Various high performance UV NLO crystals such as $Li_4Sr(BO_3)_2$ (2.0 × KDP),[6] $Cs_2B_4SiO_9$ (4.6 × KDP),[7] $Ba_3(ZnB_5O_{10})PO_4$ (4.0 × KDP),[8] $LiCs_2PO_4$ (2.6 × KDP),[9] $Na_4La_2(CO_3)_5$ (3.0 × KDP),[10] $Ca_2Na_3(CO_3)_3F$ (3.0 × KDP),[11] and $RE(OH)_2NO_3$ (RE = La (5 × KDP), Y (5.5 × KDP), and Gd (5.6 × KDP))[12] have been reported, among which borates have proven to be excellent candidates due to their relatively large SHG responses, wide ultraviolet transmittance and high optical damage thresholds.[13-18] Borates may exhibit rich structural chemistry; polyborate anions from $[B_3O_3(OH)]^{2+}$ to $[B_{24}O_{42}(OH)_2]^{14-}$ are constructed via corner- and/or edge-sharing oxygen atoms of BO_3 triangles and BO_4 tetrahedra.[19-23] Alkali and alkaline-earth metal−oxygen bonds are favorable for the transmission of UV light because there are no d−d electron transitions in this region[24-26] and, to date, commercially manufactured UV NLO crystals are dominated by metal borates such as LiB_3O_5 (LBO),[27] β-BaB_2O_4 (BBO),[28] $CsLiB_6O_{10}$ (CLBO),[29] and $KBe_2BO_3F_2$ (KBBF).[30]

Crystalline UV NLO borates can be prepared through hydrothermal methods, flux syntheses, high-temperature solid-state reactions and room-temperature self-assembly processes.[21-35] Among these possibilities, hydrothermal syntheses are milder and possess the merits of both kinetic and thermodynamic control during the reaction.[36] Consequently, numerous crystalline UV NLO borates, such as $Ca_2[B_5O_9]\cdot(OH)\cdot H_2O$,[37] $K_3B_3O_4(OH)_4\cdot 2H_2O$,[38] $Ba_2B_6O_9(OH)_4$,[39] and $LiBa_3(OH)(B_9O_{16})[B(OH)_4]$,[40] have been prepared through hydrothermal methods. Previous work has demonstrated that synthetic conditions such as pH and concentration of boron in aqueous solution may strongly affect the structures of the resultant metal borates.[41,42]

We have recently focussed on developing facile syntheses of UV NLO borates. In the present study, mixed-alkali-metal borates were prepared by a facile solvothermal method: three sodium potassium borates, namely $NaK(B_5O_8)(OH)\cdot H_2O$ (**1**), $NaK_6[(B_4O_5)(OH)_4]_3(OH)\cdot C_2H_5OH$ (**2**), and $Na_{0.33}K_{1.67}(B_4O_5)(OH)_4\cdot 3H_2O$ (**3**),[43] were obtained by adjusting the solvothermal reaction solvents, with **1** and **2** possessing 3D centrosymmetric frameworks and **3** possessing an acentric skeleton. We report herein details of the solvothermal syntheses and optical properties of **1**-**3**, the thermal behavior and crystal structures of **1**-**2**, and NLO properties and theoretical studies of **3**.

Experimental

Reagents

All reagents including $Na_2B_4O_7\cdot 10H_2O$ (99.5%), $K_2B_4O_7\cdot 4H_2O$ (99.5%), KNO_3 (99.0%), CH_3OH (99.5%), C_2H_5OH (99.5%),

[a] China-Australia Joint Research Center for Functional Molecular Materials, School of Chemical and Material Engineering, Jiangnan University, Wuxi 214122, P. R. China.
[b] Research School of Chemistry, Australian National University, Canberra, ACT 2601, Australia.

†Electronic Supplementary Information (ESI) available: X-ray crystallographic file in CIF format (CSD-431768 for 1 and CSD-431769 for 2), additional structures, selected bond distances and angles, simulated and measured powder XRD patterns, IR spectra, TGA, diffuse reflectance absorption spectra and theoretical calculations. For ESI and crystallographic data in CIF or other electronic format see DOI: 10.1039/x0xx00000x

and *N,N*-dimethylethanolamine (DMEA, 99.5%) were purchased commercially and used without further purification.

Synthesis of $NaK(B_5O_8)(OH)\cdot H_2O$ (1)

A mixture of $Na_2B_4O_7\cdot 10H_2O$ (0.381 g, 1.00 mmol), $K_2B_4O_7\cdot 4H_2O$ (0.610 g, 2.00 mmol), and KNO_3 (0.202 g, 1.00 mmol) was added to a mixed solvent of H_2O (1 mL) and CH_3OH (5 mL). The resulting mixture was stirred for 30 min, and the resultant solution was sealed in a 20 mL Teflon-lined stainless steel autoclave, heated at 210 °C for 72 h, and then slowly cooled to room temperature at a rate of 4 °C/h. The initial and final pH values were 8.4 and 8.3, respectively. Colorless block crystals of $NaK(B_5O_8)(OH)\cdot H_2O$ (**1**) were collected and dried in air. Yield: 72% (based on Na). IR data (KBr, cm^{-1}): 3379 m (br, m), 3147 m, 1463 m, 1384 m, 1340 m, 1263 w, 1128 s, 1043 s, 1003 s, 943 m, 825 s, 705 m, 630 w, 565 w, 540 w.

Synthesis of $NaK_6[(B_4O_5)(OH)_4]_3(OH)\cdot C_2H_5OH$ (2)

The same procedure was employed to synthesize **2** except using a mixed solvent of H_2O (1 mL) and C_2H_5OH (5 mL). The initial and final pH values were 8.2 and 8.0, respectively. Colorless block crystals of $NaK_6[(B_4O_5)(OH)_4]_3(OH)\cdot C_2H_5OH$ (**2**) were obtained. Yield: 61% (based on Na). IR data (KBr, cm^{-1}): 3380 m (br, m), 3126 m, 1467 m, 1384 w, 1336 m, 1257 w, 1128 s, 1043 s, 1004 s, 943 m, 825 s, 703 m, 659 w, 576 w, 540 w.

Synthesis of $Na_{0.33}K_{1.67}(B_4O_5)(OH)_4\cdot 3H_2O$ (3)

The same procedure was employed to synthesize **3** except employing a mixed solvent of H_2O (4 mL) and DMEA (2 mL). The initial and final pH values were 9.5 and 9.2, respectively. Colorless block crystals of $Na_{0.33}K_{1.67}(B_4O_5)(OH)_4\cdot 3H_2O$ (**3**) were obtained. Yield: 54% (based on Na).

Structural Determinations

Crystal structure determinations of **1** and **2** were performed on a Bruker D8 VENTURE CMOS X-ray diffractometer equipped with graphite-monochromated Mo-Kα radiation (λ = 0.71073 Å) at room temperature. Data collection and reduction were performed using APEX II software. Multi-scan absorption corrections were applied to both data sets using the APEX II program. Both structures were solved by direct methods and refined on F^2 by full-matrix least-squares methods using the *SHELXTL-97* software package.[44-45] All non-hydrogen atoms were refined with anisotropic displacement parameters except atoms C1, C2 and O7 in **2**, which were refined with "ISOR" constraints. O(9) in **1** and O(4), O(5) and O(6) in **2** were assigned as hydroxyl groups, and O(10) in **1** were assigned as water molecules on the basis of the requirements of charge balance and bond valence calculations. In **2**, the C_2H_5OH molecules are disordered. By using PLATON, both structures were also checked for possible missing symmetry, none being found.[46] Crystal data and structure refinement information for both compounds are summarized in Table 1. Selected important bond distances (Å) and angles (deg) are listed in Table S1 and Table S2 (ESI†).

IR Spectra

FT-IR spectra of both crystals were recorded on a Nicolet 360 FT-IR instrument (as KBr discs) in the range 500−4000 cm^{-1} with a resolution of 4 cm^{-1}. 5 mg of each sample was mixed thoroughly with 200 mg of oven-dried KBr.

UV-Vis-NIR Diffuse Reflectance Spectra

Optical diffuse-reflectance spectra were performed with a UV-3600 Plus UV-Vis-NIR spectrophotometer at room temperature. A $BaSO_4$ plate was used as a standard (100% reflectance). The absorption spectra were calculated from the reflectance spectra using the Kubelka-Munk function $\alpha/S = (1 - R)^2/2R$, where α is the absorption coefficient, S is the scattering coefficient that is practically wavelength-independent when the particle size is larger than 5 μm, and R is the reflectance.[47]

Thermogravimetric Analyses

Thermogravimetric analysis (TGA) experiments were carried out on a TGA/1100SF instrument at a heating rate of 10 °C/min under a nitrogen atmosphere.

Powder X-ray Diffraction Studies

Powder X-ray diffraction (P-XRD) patterns were recorded using Cu-Kα radiation on a Bruker D8 X-ray diffractometer in

Table 1 Crystal and structure refinement data for **1** and **2**. [a]

Formula	Compound **1**	Compound **2**
Formula weight	279.16	894.48
Temperature	293(2) K	293(2) K
Crystal system	triclinic	trigonal
Space group	$P\bar{1}$	$R\bar{3}c$
a (Å)	6.6230(5)	11.0685(2)
b (Å)	6.6306(5)	11.0685(2)
c (Å)	11.2044(9)	40.5755(19)
α (°)	78.620(3)	90
β (°)	76.714(3)	90
γ (°)	60.612(2)	120
V (Å^3)	415.17(6)	4305.0(3)
Z	2	6
ρ_{calc}/ g·cm^{-3}	2.233	2.070
μ / mm^{-1}	0.735	1.041
F(000)	276	2688
θ (deg)	3.54-26.00	3.68-26.39
Limiting indices	-8≤h≤8, -8≤k≤8, 13≤l≤13	-13≤h≤13, -13≤k≤13, -48≤l≤50
R_{int}	0.0244	0.0227
Reflections collected / unique	9277/1617	7741/978
GOF on F^2	1.106	1.112
R_1/ wR_2 ($I > 2\sigma(I)$)[a]	0.0529/0.1445	0.0351/0.1037
R_1/ wR_2 (all data)	0.0543/0.1449	0.0382/0.1067
Largest diff. peak and hole (e. Å^{-3})	0.857 and -0.527	0.949 and -0.269

[a] $R_1 = \sum||F_o| - |F_c||/\sum|F_o|$; $wR_2 = [\sum w(F_o^2 - F_c^2)^2]/\sum w(F_o^2)^2]^{1/2}$

the angular range 2θ = 5−70° with a step size of 0.02° and a fixed time of 1 s/step.

Second-Order NLO Measurements

Measurements of the powder frequency-doubling effect were carried out by the method of Kurtz and Perry,[48] employing a Q-switched Nd:YAG laser at 1064 nm and frequency doubling to 532 nm for visible and ultraviolet SHG, respectively. The crystal samples were ground and sieved into seven distinct particle size ranges (<26, 26−50, 50−74, 74−105, 105−150, 150−200 and 200−280 μm), which were pressed into disks with diameters of 6 mm that were put between glass microscope slides and secured with tape in a 1 mm thick aluminium holder. Crystalline KDP and BBO were also ground and sieved into the same particle size ranges and used as the reference.

Computational Methods

All electronic structure calculations were performed using the VASP code[49] in the framework of density functional theory (DFT). The generalized gradient approximation (GGA) function of Perdew-Burke-Ernzerhof (PBE)[50] was employed. A plane wave basis with a frozen-core projector-augmented wave (PAW)[51,52] potential and a plane wave cut-off energy of 400 eV was used. A grid of 5 × 5 × 4 Monkhurst-Pack *k*-points was used for the self-consistent-field convergence of the total electronic energy. The Fermi level was set at zero as the energy reference.

Results and discussion

Syntheses

Three types of crystals in the mixed-alkali-metal borates system have been synthesized by employing different polar solvents under solvothermal conditions. Scheme **1** summarizes the reaction conditions and the structural features of **1** − **3**,

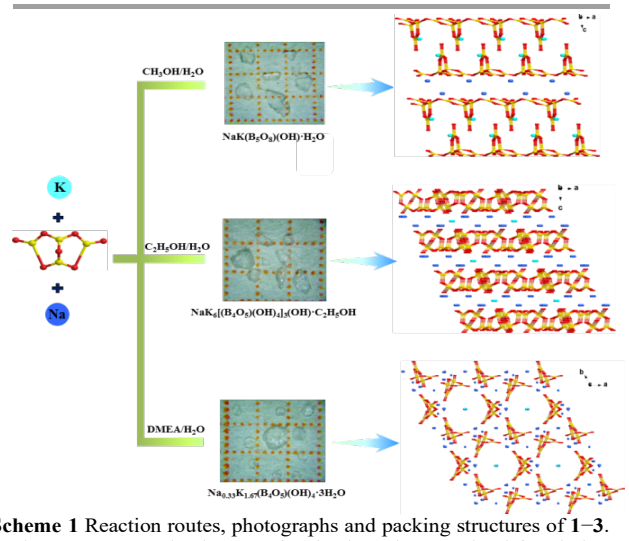

Scheme 1 Reaction routes, photographs and packing structures of **1**–**3**. Hydrogen atoms and solvent molecules have been omitted for clarity. Color codes: B gold, O red, Na turquoise, K light blue.

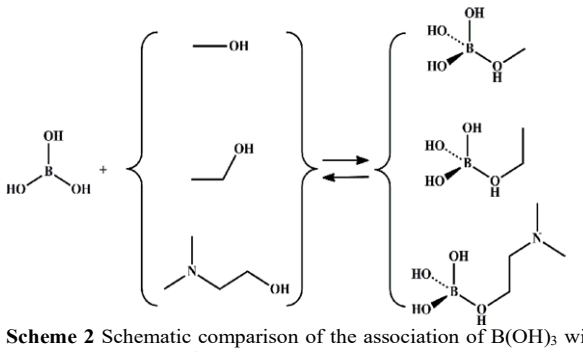

Scheme 2 Schematic comparison of the association of $B(OH)_3$ with CH_3OH, C_2H_5OH and DMEA.

including the new compounds **1** and **2**. By using CH_3OH/H_2O as solvent, compound **1** was obtained as colorless block crystals in 72% yield (based on Na). Employing C_2H_5OH/H_2O as the solvent afforded **2** as colorless block-like crystals in ~61% yield (based on Na). When C_2H_5OH/H_2O was replaced by DMEA/H_2O, block-like colorless crystals of **3** were obtained in ~54% yield (based on Na). All three of these crystalline materials are stable under ambient conditions for several months.

It is well-known that the structures of borates are very sensitive to the synthetic conditions (including reaction medium, pH, concentration of boron, reaction temperature, and reaction time).[53] In the present study, the reaction medium plays a key role in promoting the crystallization of the three borates. There were no crystals formed in our initial attempt using H_2O as solvent, but in contrast, the mixed polar solvents promoted the crystallization of **1**-**3**. Under these conditions, tetrahydroxyborate ion was formed as follows: $B_4O_7^{2-} + 7H_2O \rightarrow 2H_3BO_3 + 2B(OH)_4^-$. In combination with CH_3OH, C_2H_5OH and DMEA, the boric acid forms three different boric esters that are readily hydrolyzed to the corresponding alcohol and boric acid under solvothermal conditions (Scheme 2). Although they are unstable intermediates, [54,55] it is possible that these three different boric esters may influence the structural variations found from the sealed reactions.

Crystal Structures

*Crystal Structure of **1***. Single-crystal X-ray structure analysis revealed that **1** crystallizes in a centrosymmetric triclinic crystal system with space group $P\bar{1}$. In the metal borate crystal, the primary building units (PBUs), the pentaborate anions $[B_5O_{11}]^{7-}$, are composed of three BO_3 triangles (Δ) and two BO_4 tetrahedra (T) linked via bridging O atoms (Fig. 1a). According to the classification of Christ *et al.*,[56] the shorthand notation for the $[B_5O_{11}]^{7-}$ cluster is [5:(3Δ + 2T)], which is different from that of the known penta-borate cluster units of B_5O_{12} [5:(2Δ + 3T)][57] and B_5O_{10} [5:(4Δ + T)][58]. Each $[B_5O_{11}]^{7-}$ PBU is attached to four adjacent PBUs via B(1)–O(1)–B(2) and B(1)–O(7)–B(3) linkages (Fig. 1b). Further connectivity of the $[B_5O_{11}]^{7-}$ PBUs through their vertices yields a 2D-layered framework in the *ab* plane with 9-membered-rings (Fig. 1c). The 9-membered-rings have O···O distances in the range 5.30 Å to 6.68 Å (Fig. 1d).

The asymmetric unit of **1** contains one K atom, one Na atom, five B atoms, eight O atoms, one OH group and one H_2O

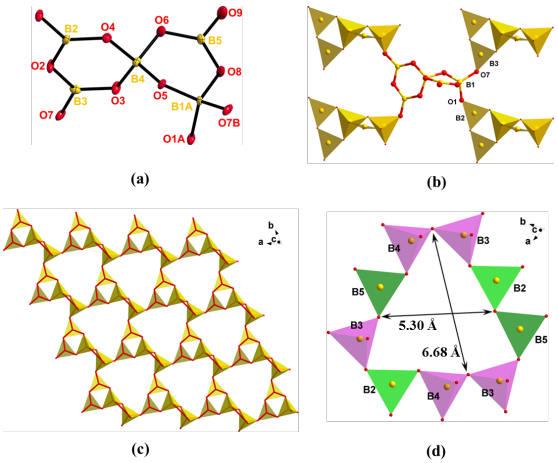

Fig. 1 (a) $[B_5O_{11}]^{7-}$ cluster unit, symmetry code: (A) x, 1 + y, z; (B) 1 + x, y, z, (b) polyhedral linking mode of $[B_5O_{11}]^{7-}$ PBU and four adjacent PBUs in **1**, (c) view of the 2D B–O layer along the *c*-axis, and (d) the 9-membered rings in the structure viewed down the *c*-axis. The BO_3 and BO_4 units are shown as green and purple, respectively.

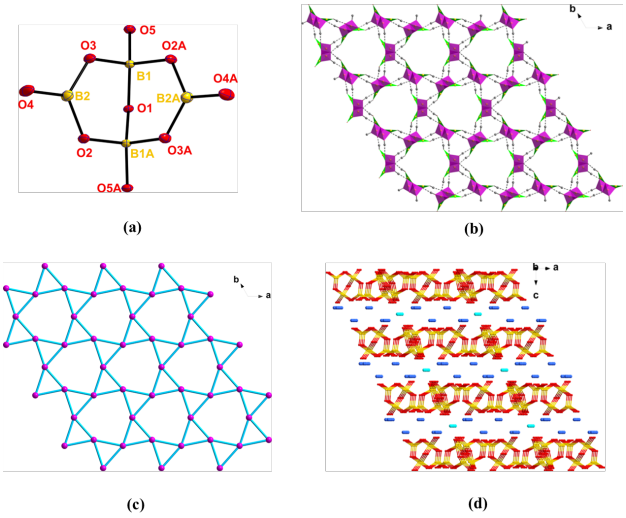

Fig. 3 (a) $[B_4O_9]^{6-}$ cluster unit, symmetry code: (A) 1.33333–x, 0.66667–x+y, 1.16667–z, (b) view of the 2D supramolecular framework constructed via hydrogen bonds, (c) topological view of the 2D 4-nodal net with the Schläfli symbol $\{3^2.6^2\}$; the purple balls represent the four-connected nodes, and (d) view of the packing structure of **2** along the *b*-axis. Hydrogen atoms have been omitted for clarity. Color codes: BO_3 triangle, green, BO_4 tetrahedron, purple, B gold, O red, Na turquoise, K light blue.

molecule (Fig. S1 in the ESI†). The B atoms adopt two coordination modes in the BO_3 triangle (B2, B3 and B5) and BO_4 tetrahedron (B1 and B4). The B–O bond distances fall in the ranges 1.339(6)–1.398(6) Å for the BO_3 triangles and 1.420(6)–1.517(6) Å for the BO_4 tetrahedrons. The O–B–O angles of the BO_3 and BO_4 groups are in the ranges 116.0(4)–124.0(4)° and 104.7(4)–113.5(4)°, respectively. These values are comparable to those of previously reported borate compounds.[59-61]

The K and Na polyhedra form their own frameworks and balance the charge of the 2D B–O layers. The K ion is eight-coordinate and located in the cavity of the nine-membered boron rings within the B–O layer (Figs. 2a and 2c). The Na ion is six-coordinate and is bridged via two H_2O molecules, forming a sodium dimer located between two K–B–O layers (Figs. 2b and 2c). Each adjacent K–O layer is pillared by sodium dimers forming a 3D open framework (Fig. 2d). There are weak H-bonding interactions between adjacent B–O layers, with O···O distances in the range 2.8429-2.8961 Å (Fig. S2 and Table S3 in the ESI†). Bond valence sum (BVS) calculations

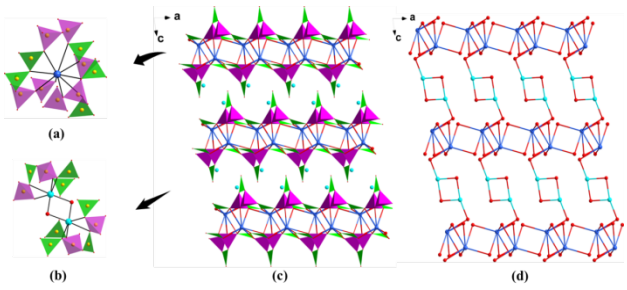

Fig. 2 (a) View of the coordination environments of the K atoms, (b) view of the coordination environments of the dimer-containing Na atoms, (c) view of the packing structure of **1** along the *b*-axis, and (d) the K and Na atoms in the interconnected 3D framework. Color codes: BO_3 triangle, green, BO_4 tetrahedron, purple, O red, Na turquoise, K light blue.

for atoms K(1), Na(1) and B(1) to B(5) gave values of 1.27, 1.15, 3.01, 3.04, 3.05, 3.05 and 3.04, respectively, consistent with oxidation states of +1 for K, +1 for Na and +3 for B, as expected.[62,63]

Crystal Structure of ***2****.* Compound **2** crystallizes in the trigonal crystal system with centrosymmetric space group $R\bar{3}c$. The asymmetric unit of **2** contains one Na ion, one K ion, two B atoms, four O atoms, two OH groups and one C_2H_5OH molecule (Fig. S3 in the ESI†). The PBU in **2** is a $[B_4O_9]^{6-}$ cluster that consists of two BO_3 triangles and two BO_4 tetrahedra (Fig. 3a), which can be written as [4:(2Δ + 2T)] in the classification of Christ *et al.* The B–O distances range from 1.370(3) to 1.374(3) Å and the O–B–O bond angles are 118.0(2)–122.4(2)° for the BO_3 triangles, while the B–O distances are in the range 1.449(2)–1.496(3) Å and the O–B–O bond angles are 108.31(17)–110.59(17)° for the BO_4 tetrahedra. The polyanions $[B_4O_9]^{6-}$ are further connected by eight hydrogen bonds between four adjacent PBUs, forming 2D supramolecular layers in the *ab* plane (Fig. 3b and Table S4). In other words, defining the $[B_4O_9]^{6-}$ PBU as a four-connected node and H(4) and H(5) as connectors, the anionic framework can be regarded as possessing 4-connected net topology with the Schläfli symbol $\{3^2.6^2\}$ (Fig. 3c). Moreover, terminal hydroxyls exist in the layers and point to the same sides with the same orientations (Fig. S4 in the ESI†).

The K and Na ions fill the space between the adjacent layers, balance the charge, and hold the layers together via connections with the O atoms (Fig. 3d). The 8-coordinated K–O and 6-coordinated Na–O bond distances vary from 2.737(2) to 3.096(2) Å and from 2.331(6) to 2.334(3) Å, respectively (Fig. S5 in the ESI†). The bond valence sum (BVS) calculations give values of 3.04, 3.00, 1.10 and 1.42 for B(1), B(2), K(1) and

Na(1) atoms, which are consistent with the expected valences.[62,63]

Crystal Structure of 3. Compound **3** crystallizes in the acentric space group $P\bar{6}2c$. The asymmetric unit of **3** contains one Na ion, four K ions, two B atoms, and eight O atoms. The B1 atoms are bonded to three O atoms to form the BO_3 triangles, and B2 are connected to four oxygens to form the BO_4 tetrahedra. The BO_3 triangles and BO_4 tetrahedra are then linked by an oxygen vertex forming the isolated $[B_4O_9]^{6-}$ anion groups (Fig. S6a in the ESI†). The polyanion groups are connected by eight hydrogen bonds to form a quasi-lamellar structure in the *ab* plane (Fig. S6b in the ESI†). The K cations fill in the voids between these layers and the Na cations are located at the center of the six-membered boron rings. The connectivity of the K−O and Na−O bonds leads to the construction of a 3D supramolecular framework (Figs. S6c and S6d in the ESI†).

Framework condensation: The combinations of anionic borate groups and alkali metal ions have resulted in a wide variety of open-framework inorganic borates. The reasons for incorporating alkali metals are as follows: (1) alkali metals have flexible coordination geometries that may result in diverse crystal structures; and (2) alkali metals may facilitate a wide UV transparency and may therefore be promising metal sources in the design of UV nonlinear optical materials. Many polyborate anions, such as $[B_3O_3(OH)_4]^{2-}$, $[B_4O_7(OH)_2]^{4-}$, $[B_5O_7(OH)_2]^{3-}$, and $[B_6O_9(OH)_4]^{4-}$, can be constructed from borate solutions. Anionic borates and alkali metal ions therefore afford a myriad of possibilities in combination with promising optical properties.

Charge balance and the host-guest arrangement are two key factors influencing the three different frameworks of **1**, **2** and **3**. The different frameworks of **2** and **3** are achieved by adjusting the ratio of K and Na ions per molecule, not by changing the framework of the host $[B_4O_9]^{6-}$ clusters. In addition, the guest cations acted as structure-directing agents with the polyborate anionic framework.

Powder X-ray Diffraction

The simulated and experimental PXRD patterns of the three compounds are depicted in Fig. S7 (ESI†). Most peak positions of the simulated and experimental patterns are in good agreement, indicating the phase purity of the products. The differences in intensity may be due to the preferred orientation of the powder samples.

IR Measurements

Fig. S8 (ESI†) presents the IR spectra of **1** and **2**. The two figures exhibit some similar characteristics. The broad absorption band at ca. 3350 cm^{-1} confirms the presence of hydroxyl groups and water molecules.[64,65] The strong absorption bands in the range 1250–1500 cm^{-1} are assigned to asymmetric stretching vibrations of the BO_3 groups, while the bands centered at 1130 and 900 cm^{-1} are likely to be the asymmetric and symmetric vibrations of the BO_4 groups, respectively. The bending vibrations of BO_3 and BO_4 are seen at 500–800 cm^{-1}. These assignments are consistent with the results obtained from the single-crystal X-ray structural analyses.

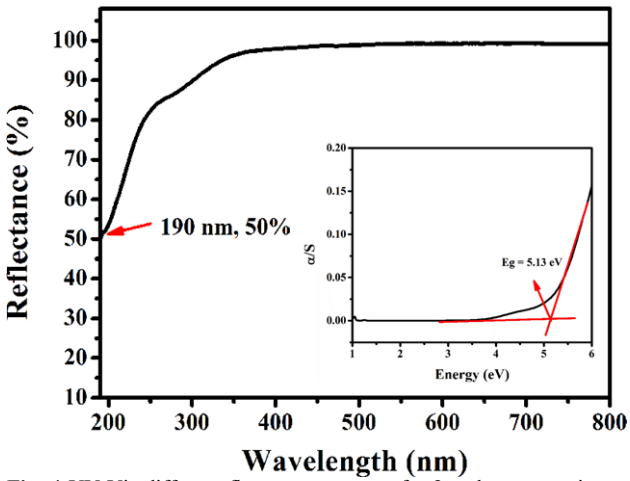

Fig. 4 UV-Vis diffuse reflectance spectrum for **3** and an approximate band gap of 5.13 eV.

UV-Vis-NIR Diffuse reflectance spectra

The UV-Vis-NIR diffuse reflectance spectra for **1**, **2** and **3** are shown in Figs. 4 and S9 (ESI†). The spectra of **1** and **2** indicate that the optical band gaps for the two compounds are ca. 5.06 eV and 5.07 eV, respectively, corresponding to the UV cutoff edges at ~245 nm. This suggests that both crystals have wide transparency ranges from the UV to the NIR (Figs. S9a and S9b in the ESI†). Similar to these two compounds, the optical diffuse reflectance spectrum of **3** reveals that its band gap is ca. 5.13 eV with a UV cutoff edge of 242 nm (Figs. 4 and S9c in the ESI†). The diffuse reflectance spectrum of **3** indicates that the absorption edge is below 190 nm, similar to other UV NLO borates.[38,66] All three compounds therefore have potential for applications in the UV.

Thermal Stability

Thermogravimetric analysis (TGA) (Fig. S10a in the ESI†) shows that **1** is stable up to 230 °C, with the weight loss occurring in two steps over the range 230–750 °C under a nitrogen atmosphere. The first step, a weight loss of approximately 6.40% in the range 230–600 °C, corresponds to the removal of the H_2O molecule (calculated value 6.45%). The second step results in a weight loss of about 3.33% (calculated value 3.25%) in the range 600–750 °C, and is assigned to the condensation of the hydroxyl groups. The TGA curve (Fig. S10b in the ESI†) of **2** also has a two-step weight loss; the minor weight loss of 5.09% (calculated value 5.15%) in the range 75-190 °C is due to the loss of C_2H_5OH, while in the second stage (190–450 °C), the weight loss is tentatively attributed to the release of 6.5 H_2O molecules. The observed weight loss of 13.01% matches well with the calculated value (13.09%). The final residuals of the two compounds were

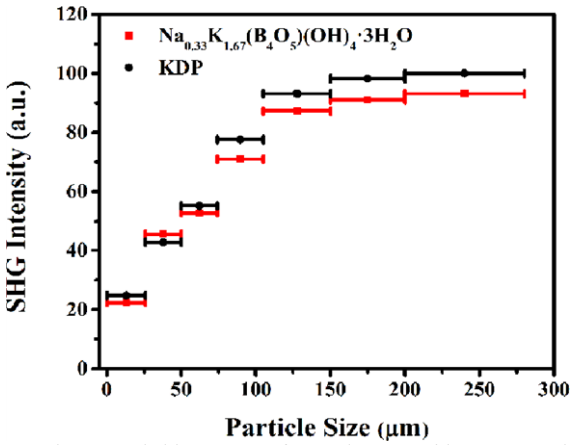

Fig. 5 Phase-matchable curves of **3** and KDP with 1064 nm laser radiation.

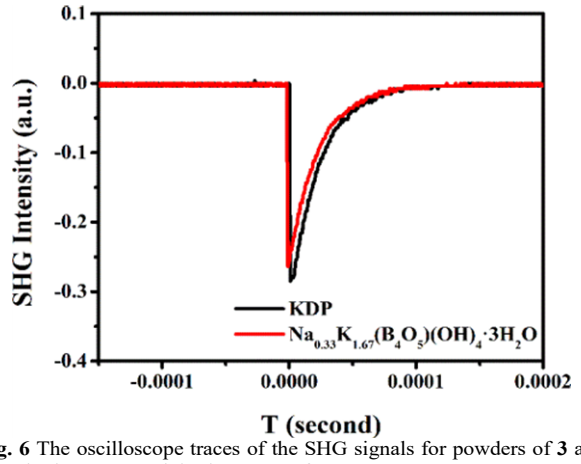

Fig. 6 The oscilloscope traces of the SHG signals for powders of **3** and KDP in the same particle size range of 150-200 μm.

examined, but no matching compounds could be identified from the powder XRD patterns.[67]

SHG Properties

The noncentrosymmetric crystal structure of the mixed alkali-metal borate **3** encouraged us to examine its SHG properties. SHG measurements were conducted using an incident laser at λ = 1064 nm. KDP was selected as the reference for visible SHG measurements. The SHG intensity of **3** increases with increasing particle size before it reaches a maximum that is independent of particle size (Fig. 5), indicating that **3** is type I phase-matchable. Compound **3** exhibits a moderate SHG response efficiency (ca. 0.94 times that of KDP) in the particle size range 150−200 μm (Fig. 6). Its value is comparable to those of some previously reported alkaline-earth metal borates, e.g. $Li_4Cs_3B_7O_{14}$ (0.5 × KDP),[68] $Li_3Cs_2B_5O_{10}$ (0.5 × KDP)[69] and $LiNaB_4O_7$ (0.15 × KDP)[70]. With the incident laser at 532 nm, the SHG intensity of **3** shows a weak SHG response compared with BBO in the same particle size range (Fig. S11 in the ESI†). The NLO optical properties can be preliminarily explained from the structural configuration of **3**. From anionic

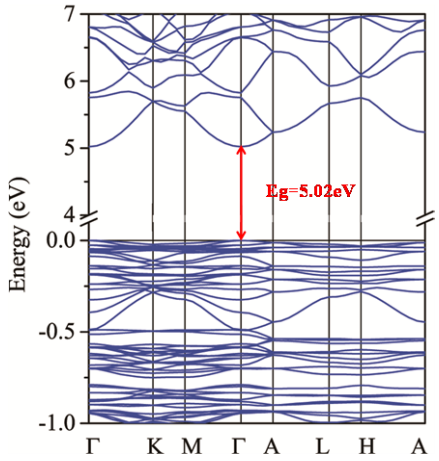

Fig. 7 Calculated band structure of **3**.

group theory,[71-73] the π-conjugated system of triangular BO_3 groups, rather than BO_4 groups, should be responsible for the larger SHG effect. In the structure of **3**, the BO_3 groups are aligned in a nearly anti-parallel orientation (Figure S14), which is an unfavorable pattern for generating a large SHG effect. Taking the number density of the BO_3 groups into account, the densities of the BO_3 groups are 0.0069 per unit volume for **I**, which is smaller than that of KBBF (0.00946 per unit volume). In the present case, and considering also the distorted KO_6 polyhedral NLO-active units,[74] we can conclude that the moderate SHG response of **3** mainly originates from the cooperative action of the distorted KO_6 polyhedra and the polarized BO_3 triangles. As a result, one would expect that the overall SHG efficiency of **3** would remain moderate, and this was confirmed by SHG measurements.

Theoretical Studies

To better understand the band structure features of **3**, first-principles calculations of the electronic structure was performed. From the calculated band structure (Fig. 7), the conduction band minimum (CBM) and the valence band maximum (VBM) are located at point Γ with a band gap of 5.02 eV, indicating that **3** belongs to a direct band gap compound. The value is slightly less than the experimental value of 5.13 eV due to the limitation of the DFT methods, primarily a result of the exchange correlation energy being inaccurately calculated.[75]

It is well-known that the valence electrons play an important role in most optical properties of a compound, which are dominated by the band structure in the vicinity of the Fermi level. The contributions of atoms and their orbitals to other bands around the Fermi level can be seen from the density of state (DOS) plots in Fig. 8. It is clear that the valence band from –8 eV to the Fermi level is mainly composed of O-2p, H-1s and B-2p orbitals, and a strong hybridization between oxygen and the neighboring atoms is exhibited. The conduction bands are dominated by mixing of O-2p, B-2p, H-1s and K-4s

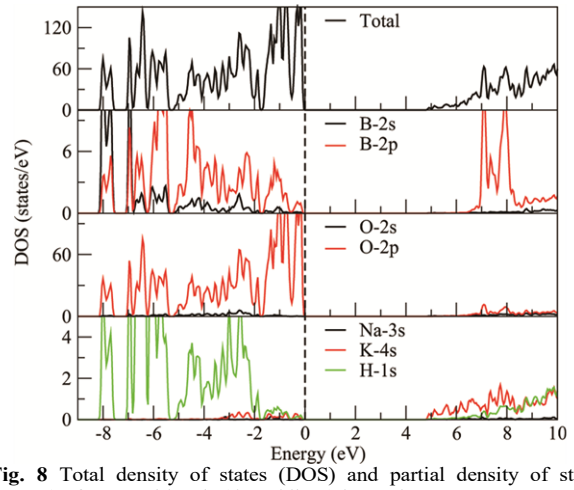

Fig. 8 Total density of states (DOS) and partial density of states (PDOS) of **3**. Fermi levels (dotted lines) located at zero.

orbitals. It is clear that the bands around the Fermi level are comprised predominantly of K, B, O, and H orbitals, which indicates that the K-O, B-O, and H-O bonds are the dominant active units influencing the optical properties.

The electron densities of VBM and CBM at Γ for **3** are shown in Fig. S12 (ESI†). The VBM of **3** is composed of O-2p states localized at the O atom, while the CBM is significantly delocalized, consisting mainly of 2s states from the O atoms together with states of potassium. These suggest that the K, B, and O atoms have a positive effect on the band gap.

Conclusions

In summary, a series of mixed-alkali-metal borate species have been synthesized by solvothermal methods using various organic polar solvents. Interestingly, the different solvent systems (CH_3OH/H_2O, C_2H_5OH/H_2O and DMEA/H_2O) employed in the syntheses resulted in diversity in the framework structures. The structure of **1** features a 2D-layered framework constructed by $[B_5O_{11}]^{7-}$ primary building units, assembled into to a 3D framework by K^+ and Na^+ cations, while the structure of **2** consists of isolated $[B_4O_9]^{6-}$ primary building units, which are interconnected via K^+, Na^+ cations and H-bonding interactions to generate a 3D supramolecular framework. The acentric crystal **3** exhibits a short UV cutoff edge (~ 242 nm) and is phase-matchable with a moderate SHG response (ca. 0.94 × KDP). These features make **3** a promising UV NLO material. Further research developing mixed-alkali-metal borates under solvothermal conditions for UV NLO materials is currently in progress.

Acknowledgements

This research was financially supported by the National Natural Science Foundation of China (No. 51432006, 50925207, and 51172100), the Ministry of Science and Technology of China (No. 2011DFG52970), the Ministry of Education of China for the Changjiang Innovation Research Team (No. IRT13R24), and the Ministry of Education and the State Administration of Foreign Experts Affairs for the 111 Project (No. B13025). M.G.H. thanks the Australian Research Council for support.

References

1 M. Lee, H. E. Katz, C. Erben, D. M. Gill, P. Gopalan, J. D. Heber, D. J. McGee, *Science*, 2002, **298**, 1401.
2 D. Cyranoski, *Nature*, 2009, **457**, 953.
3 T. C. Lin, J. M. Cole, A. P. Higginbotham, A. J. Edwards, R. O. Piltz, J. Perez-Moreno, J. Y. Seo, S. C. Lee, K. Clays, O. P. Kwon, *J. Phys. Chem. C*, 2013, **117**, 9416.
4 Y. Y. Li, P. F. Liu, H. Lin, M. T. Wang, L. Chen, *Inorg. Chem. Front.*, 2016, **3**, 952.
5 Y. H. Kim, T. T. Tran, P. S. Halasyamani, K. M. Ok, *Inorg. Chem. Front.*, 2015, **2**, 361.
6 S. G. Zhao, P. F. Gong, L. Bai, X. Xu, S. Q. Zhang, Z. H. Sun, Z. S. Lin, M. C. Hong, C. T. Chen, J. H. Luo, *Nature Commun.*, 2014, **5**, 4019.
7 H. P. Wu, H. W. Yu, S. L. Pan, Z. J. Huang, Z. H. Yang, X. Su, K. R. Poeppelmeier, *Angew. Chem. Int. Ed.*, 2013, **52**, 3406.
8 H. W. Yu, W. G. Zhang, J. H. Young, J. M. Rondinelli, P. S. Halasyamani, *Adv. Mater.*, 2015, **27**, 7380.
9 L. Li, Y. Wang, B. H. Lei, S. J. Han, Z. H. Yang, K. R. Poeppelmeier, S. L. Pan, *J. Am. Chem. Soc.*, 2016, **138**, 9101.
10 M. Luo, G. X. Wang, C. S. Lin, N. Ye, Y. Q. Zhou, W. D. Cheng, *Inorg. Chem.*, 2014, **53**, 8098.
11 M. Luo, Y. X. Song, C. S. Lin, N. Ye, W. D. Cheng, X. F. Long, *Chem. Mater.*, 2016, **28**, 2301.
12 Y. X. Song, M. Luo, C. S. Lin, N. Ye, *Chem. Mater.*, DOI: 10.1021/acs.chemmater.6b05119
13 R. H. Cong, Y. Wang, L. Kang, Z. Y. Zhou, Z. S. Lin, T Yang, *Inorg. Chem. Front.*, 2015, **2**, 170.
14 Y. N. Xia, C. T. Chen, D. Y. Tang, B. C. Wu, *Adv. Mater.*, 1995, **7**, 79.
15 C. T. Chen, S. Y. Luo, X. Y. Wang, G. L. Wang, X. H. Wen, H. X. Wu, X. Zhang, Z. Y. Xu, *J. Opt. Soc. Am. B*, 2009, **26**, 1519.
16 S. C. Wang, N. Ye, W. Li, D. Zhao, *J. Am. Chem. Soc.*, 2010, **132**, 8779.
17 H. W. Yu, J. Cantwell, H. P. Wu, W. G. Zhang, *Cryst. Growth Des.*, 2016, **16**, 3976.
18 H. Yang, C. L. Hu, X. Xu, J. G. Mao, *Inorg. Chem.*, 2015, **54**, 7516.
19 H. Huppertz, *Chem. Commun.*, 2011, **47**, 131.
20 S. Wang, E. V. Alekseev, W. Depmeierc, T. E. Albrecht-Schmitt, *Chem. Commun.*, 2011, **47**, 10874.
21 S. C. Neumaira, R. Kaindl, H. Huppertz, *J. Solid State Chem.*, 2012, **185**, 1.
22 M. Yang, J. H. Yu, J. C. Di, J. Y. Li, P. Chen, Q. R. Fang, Y. Chen, R. R. Xu, *Inorg. Chem.*, 2006, **45**, 3588.
23 H. R. Tian, W. H. Wang, Y. E. Gao, T. T. Deng, J. Y. Wang, Y. L. Feng, J. W. Cheng, *Inorg. Chem.*, 2013, **52**, 6242.
24 H. Lin, J. N. Shen, Y. F. Shi, L. H. Li, L. Chen, *Inorg. Chem. Front.*, 2015, **2**, 298.
25 B. Sahraoui, R. Czaplicki, A. Klöpperpieper, A. S. Andrushchak, I. V. Kityk, *J. Appl. Phys.*, 2010, **107**, 113526.
26 S. G. Zhao, P. F. Gong, S. Y. Luo, L. Bai, Z. S. Lin, C. M. Ji, T. L. Chen, M. C. Hong, J. H. Luo, *J. Am. Chem. Soc.*, 2014, **136**, 8560.
27 C. T. Chen, Y. C. Wu, A. D. Jiang, B. C. Wu, G. M. You, R. K. Li, S. J. Lin, *J. Opt. Soc. Am. B*, 1989, **6**, 616.
28 C. T. Chen, B. C. Wu, A. D. Jiang, G. M. You, *Sci. Sin., Ser. B*, 1985, **28**, 235.
29 Y. Mori, I. Kuroda, S. Nakajima, T. Sasaki, S. Nakai, *Appl. Phys. Lett.*, 1995, **67**, 1818.

30 C. T. Chen, G. L. Wang, X. Y. Wang, Z. Y. Xu, *Appl. Phys. B: Lasers Opt.*, 2009, **97**, 9.
31 Y. Yang, X. Su, S. L. Pan, Z. H. Yang, *Phys. Chem. Chem. Phys.*, 2015, **17**, 26359.
32 H. W. Huang, J. Y. Yao, Z. S. Lin, X. Y. Wang, R. He, W. J. Yao, N. X. Zhai, C. T. Chen, *Angew. Chem. Int. Ed.*, 2011, **50**, 9141.
33 C. D. McMillen, J. W. Kolis, *Inorg. Chem.*, 2011, **50**, 6809.
34 L. Y. Li, G. B. Li, Y. X. Wang, F. H. Liao, J. H. Lin, *Chem. Mater.*, 2005, **17**, 4174.
35 E. L. Belokoneva, S. Yu. Stefanovich, O. V. Dimitrova, N. N. Mochenova, N. V. Zubkova, *Crystallogr. Rep.*, 2009, **54**, 814.
36 J. L. Song, C. L. Hu, X. Xu, F. Kong, J. G. Mao, *Angew. Chem. Int. Ed.*, 2015, **54**, 3679.
37 Q. Wei, J. W. Cheng, C. He, G. Y. Yang, *Inorg. Chem.*, 2014, **53**, 11757.
38 Q. Liu, X. Y. Zhang, Z. H. Yang, F. F. Zhang, L. L. Liu, J. Han, Z. Li, S. L. Pan, *Inorg. Chem.*, 2016, **55**, 8744.
39 L. Wang, S. L. Pan, L. X. Chang, J. Y. Hu, H. W. Yu, *Inorg. Chem.*, 2012, **51**, 1852.
40 C. Wu, J. L. Song, L. H. Li, M. G. Humphrey, C. Zhang, *J. Mater. Chem. C*, 2016, **4**, 8189.
41 J. L. Song, C. L. Hu, X. Xu, F. Kong, J. G. Mao, *Inorg. Chem.*, 2013, **52**, 8979.
42 J. L. Song, X. Xu, C. L. Hu, F. Kong, J. G. Mao, *CrystEngComm*, 2015, **17** 3953.
43 C. Smykalla, H. Behm, *Z. Kristallogr.*, 1988, **183**, 51.
44 G. M. Sheldrick, *SHELXS-97: Program for the Solution of Crystal Structures*; University of Göttingen, Germany, 1997.
45 G. M. Sheldrick, *SHELXL-97: Program for the Refinement of Crystal Structures*; University of Göttingen, Germany, 1997.
46 A. L. Spek, *PLATON*; Utrecht University: Utrecht, The Netherlands, 2001.
47 W. M. Wendlandt, H. G. Hecht, *Reflectance Spectroscopy*; Interscience: New York, 1966.
48 S. K. Kurtz, T. T. Perry, *J. Appl. Phys.*, 1968, **39**, 3798.
49 G. Kresse, J. Furthmuller, *Phys. Rev. B*, 1996, **54**, 11169.
50 J. P. Perdew, K. Burke, M. Ernzerhof, *Phys. Rev. Lett.*, 1996, **77**, 3865.
51 P. E. Blochl, *Phys. Rev. B*, 1994, **50**, 17953.
52 G. Kresse, D. Joubert, *Phys. Rev. B*, 1999, **59**, 1758.
53 G. X. Wang, M. Luo, N. Ye, C. S. Lin, W. D. Cheng, *Inorg. Chem.*, 2014, **53**, 5222.
54 K. Ishihara, A. Nagasawa, K. Umemoto, H. Ito, K. Saitole, *Inorg. Chem.*, 1994, **33**, 3811.
55 W. T. Donald, C. B. Thomas, *J. Am. Chem. Soc.*, 1967, **89**, 6954.
56 C. L. Christ, J. R. Clark, *Phys. Chem. Miner.*, 1977, **2**, 59.
57 Y. Z. Huang, L. M. Wu, X. T. Wu, L. H. Li, L. Chen, Y. F. Zhang, *J. Am. Chem. Soc.*, 2010, **132**, 12788.
58 C. Rong, Z. W. Yu, Q. Wang, S. T. Zheng, C. Y. Pan, F. Deng, G. Y. Yang, *Inorg. Chem.*, 2009, **48**, 3650.
59 P. Becker, *Adv. Mater.*, 1998, **10**, 979.
60 K. Iliopoulos, D. Kasprowicz, A. Majchrowski, E. Michalski, D. Gindre, B. Sahraoui, *Appl. Phys. Lett.*, 2013, **103**, 231103.
61 M. J. Polinski, D. J. Grant, S. Wang, E. V. Alekseev, J. N. Cross, E. M. Villa, W. Depmeier, L. Gagliardi, T. E. Albrecht-Schmitt, *J. Am. Chem. Soc.*, 2012, **134**, 10682.
62 I. D. Brown, D. Altermatt, *Acta Crystallogr.*, 1985, **B41**, 244.
63 N. E. Brese, M. O'Keeffe, *Acta Crystallogr.*, 1991, **B47**, 192.
64 C. McMillen, C. Heyward, H. Giesber, J. Kolis, *J. Solid State Chem.*, 2011, **184**, 2966.
65 G. C. Zhang, Z. L. Liu, J. X. Zhang, F. D. Fan, Y. C. Liu, P. Z. Fu, *Cryst. Growth Des.*, 2009, **9**, 3137.
66 Y. J. Wang, S. L. Pan, X. L. Tian, Z. X. Zhou, G. Liu, J. D. Wang, D. Z. Jia, *Inorg. Chem.*, 2009, **48**, 7800.
67 F. Y. Zhang, F. F. Zhang, J. Qun, S. L. Pan, Z. H. Yang, D. Z. Jia, *Phys. Chem. Chem. Phys.* **2015**, *17*, 10489.
68 Y. Yang, S. L. Pan, H. Y. Li, J. Han, Z. H. Chen, W. W. Zhao, Z. X. Zhou, *Inorg. Chem.*, 2011, **50**, 2415.
69 Y. Yang, S. L. Pan, X. L. Hou, C. Y. Wang, K. R. Poeppelmeier, Z. H. Chen, H. P. Wu, Z. X. Zhou, *J. Mater. Chem.*, 2011, **21**, 2890.
70 M. Mączka, A. Waśkowska, A. Majchrowski, J. Żmija, J. Hanuza, G. A. Peterson, D. A. Keszler, *J. Solid State Chem.*, 2007, **180**, 410.
71 C. T. Chen, *Sci. Sin. (Engl. Ed.)*, 1979, **22**, 756.
72 C. T. Chen, G. Z. Liu, *Annu. Rev. Mater. Sci.*, 1986, **16**, 203.
73 C. T. Chen, Y. C. Wu, R. K. Li, *Int. Rev. Phys. Chem.*, 1989, **8**, 65.
74 H. P. Wu, S. L. Pan, K. R. Poeppelmeier, H. Y. Li, D. Z. Jia, Z. H. Chen, X. Y. Fan, Y. Yang, J. M. Rondinelli, H. S. Luo, *J. Am. Chem. Soc.* **2011,** *133*, 7786–7790.
75 R. W. Godby, M. Schluter, L. J. Sham, *Phys. Rev. B: Condens. Matter Mater. Phys.*, 1987, **36**, 6497.